Novel amiloride derivatives that inhibit bacterial motility across multiple strains and stator types

MI Islam[1]*, JH Bae[1]*, T Ishida[2], P Ridone[1], J Lin[1], MJ Kelso[3,4], Y Sowa[2,5], BJ Buckley[3,4], MAB Baker[1,6].

*joint contribution

1. School of Biotechnology and Biomolecular Sciences, University of New South Wales, Sydney, NSW 2052, Australia.

2. Department of Frontier Bioscience, Hosei University, Tokyo, Japan.

3. Molecular Horizons and School of Chemistry and Molecular Bioscience, University of Wollongong, Wollongong, NSW 2522, Australia

4. Illawarra Health and Medical Research Institute, Wollongong, NSW 2522, Australia.

5. Research Center for Micro-Nano Technology, Hosei University, Tokyo, Japan.

6. CSIRO Synthetic Biology Future Science Platform, Brisbane, Australia.

Correspondence: matthew.baker@unsw.edu.au

Keywords:

Bacterial motility, bacterial flagellar motor, amiloride, sodium channel blocker, stator.

Abstract:

The bacterial flagellar motor (BFM) is a protein complex that confers motility to cells and contributes to survival and virulence. The BFM consists of stators that are ion-selective membrane protein complexes and a rotor that directly connects to a large filament, acting as a propeller. The stator complexes couple ion transit across the membrane to torque that drives rotation of the motor. The most common ion gradients that drive BFM rotation are protons (H^+) and sodium ions (Na^+). The sodium-powered stators, like those in the PomAPomB stator complex of *Vibrio* spp, can be inhibited by sodium channel inhibitors, in particular, by phenamil, a potent and widely used inhibitor. However, relatively few new sodium-motility inhibitors have been described since the discovery of phenamil. In this study, we discovered two motility inhibitors HM2-16F and BB2-50F from a small library of previously reported amiloride derivatives. Using a tethered cell assay, we showed that both HM2-16F and BB2-50F had inhibition comparable to that of phenamil effect on Na+ driven motors at matching concentrations, with an additional ability to inhibit rotation in H^+ driven motors. The two compounds did not exhibit adverse effects on bacterial growth at the motility-inhibiting concentration of 10 μM, however toxicity was seen for BB2-50F at 100 μM. We performed higher resolution measurements to examine rotation inhibition at moderate (1 μm polystyrene bead) and low

loads (60 nm gold bead) and in both the presence and absence of stators. These measurements suggested that the compounds did not inhibit rotation via direct association with the stator, in contrast to the established mode of action of phenamil. Overall, HM2-16F and BB2-50F showed reversible inhibition of motility across a range of loads, in both Na^+ and H^+ stator types, and in pathogenic and non-pathogenic strains.

Introduction:

Motility is essential for many bacteria to find nutrients and escape unfavourable conditions (1). Bacterial cells move through liquids or over moist surfaces using rotating flagella, which are driven by the bacterial flagellar motor (BFM) (2). In peritrichous bacteria such as *E. coli*, when the majority of BFMs rotate counter-clockwise, bacteria move linearly (i.e., run) and when one or more BFM rotates clockwise, the helical filament-bundle unravels and bacteria change direction (i.e., tumble) (3). The BFM contains the stator proteins (e.g., MotA and MotB in *E. coli* and PomA and PomB in *Vibrio* spp.), which form an ion transporter on the inner cell membrane, and the rotor proteins (e.g., FliG, FliM, and FliN), that are driven to rotate by torque generation between the stator and rotor (4). Rotation of the BFM is powered by translocation of specific ions (e.g., H^+ in *E. coli* and Na^+ in *Vibrio* spp.) across the cell membrane through the stator complex (4).

Beside locomotion, motility is crucial during the initial infection and colonisation processes of different pathogenic bacteria (5). Locomotion reduces repulsion between the bacterial cell wall and host tissues, promoting attachment to host cells (6). The importance of motility as a virulence factor was first noted in *Campylobacter jejuni,* when only the motile strain of *C. jejuni* was recovered from an infection site where a mixture of motile and non-motile *C. jejuni* phase variants were used to initiate infection (7). It has since been demonstrated that flagellum-mediated motility promotes the virulence of several gram-negative pathogens, such as for *Bordetella bronchiseptica, B. pertussis* (8)*, Helicobacter sp.* (9)*, Legionella pneumophila* (10), pathogenic *E. coli* strains (11), *Pseudomonas aeruginosa* (12)*, Salmonella typhimurium* (13)*,* and *Vibrio cholerae* (14)*.* Aside from host attachment, flagella also contribute to the formation of biofilms by multiple bacterial pathogens, which promote the development of persistent and chronic infections and antibiotic resistance (1).

Amiloride is a diuretic drug and well-characterised inhibitor of the Na^+ bacterial flagellar motor (15). Amiloride inhibits rotation of the sodium powered flagellar motor by blocking the translocation of Na^+ ions through the channel in a competitive and rapidly reversible manner (16). However, amiloride is of limited utility due to its weak anti-motility activity and adverse effects on other metabolic processes (17). The *N*-phenyl substituted amiloride analogue, phenamil, has been identified as a better inhibitor of sodium powered flagellar motors (17). Phenamil is markedly more potent than amiloride and shows non-competitive inhibition of bacterial motility with slow dissociation (18). Phenamil stops flagellar

rotation by binding to a site predicted to lie at the cytoplasmic face of the PomAPomB stator complex (19). Phenamil is a useful tool for flagellar research, but requires high concentrations (>20 μM) and resistant stators can arise from a single point mutation (20, 21). More potent and specific compounds may assist research into stator function and potentially offer leads for new antivirulence drugs. While classical uncouplers can be used to inhibit proton powered motors, they also have adverse effects on cells resulting from collapse of the membrane potential. For example the commonly used uncoupler, carbonyl cyanide *m*-chlorophenyl hydrazone (CCCP), is toxic to both prokaryote and eukaryote cells (22). Here, we report that two recently reported 6-substituted amiloride analogues, BB2-50F and HM2-16F(23, 24) (Fig. 1A), inhibit motility in known phenamil-resistant strains and affect both Na^+ and H^+ powered flagellar motors.

Results:

Inhibition of motility

We initially evaluated the anti-motility activity of BB2-50F and HM2-16F along with the control compounds HMA and phenamil using a tethered cell assay (Fig. 1B). We examined the effect of each compound on rotational speed at increasing concentrations (0, 1, 10, and 100 μM) against Na^+ powered stator, PomAPotB in *E. coli* SYC35 (Δ*motAmotB fliC*^{sticky}) strains. Both BB2-50F and HM2-16F inhibited rotation speed in a dose-dependent manner and showed complete inhibition at 10 μM and above (Fig. 1B). The positive control for Na^+ -inhibition, phenamil showed similar dose-dependency, with complete inhibition at 10 μM (Fig. 1B). HMA was less potent, with 65% of cells still rotating at 10 μM (Fig. 1B), in agreement with previous findings with other 5-substituted amiloride analogues (16).

We further characterised the activity of BB2-50F and HM2-16F alongside phenamil over the concentration range 0−10 μM (Fig. 1C). BB2-50F showed a 2% reduction in the number of rotating cells at 1 μM, 4% at 2.5 μM, 12% at 5 μM, 20% at 7.5 μM and 79% at 10 μM (Fig 1C). HM2-16F showed a 6% reduction in the number of rotating cells at 1 μM, 15% at 2.5 μM, 28% at 5 μM, 62% at 7.5 μM and 100% at 10 μM (Fig. 1C). In comparison, phenamil produced a 27% reduction in the number of rotating cells at 1 μM, 36% at 2.5 μM, 51% at 5 μM, 58% at 7.5 μM and 74% at 10 μM (Fig. 1C). The effect of each compound was reversed following washing with motility buffer.

Effect on bacterial growth

We measured the growth of *E. coli* SYC35 cells expressing sodium powered stators (PomAPotB) (Supplementary Fig. 1A) and proton powered stators (MotAMotB) (Supplementary Fig. 1B) in the presence of 10 μM and 100 μM BB2-50F and HM2-16F. The rate of growth in both strains was not inhibited relative to vehicle controls for either HM2-16F or BB2-50F at 10 μM (Supplementary Fig. 1).

103 However, at 100 μM the compounds differed in toxicity. HM2-16F reduced the growth rate relative to
104 control over the first five hours in both strains, but did not significantly decrease growth at 15 hr, while
105 BB2-50F completely inhibited growth at 100 μM.

106 ***Effect of Na^+ concentration on motility inhibition***

107 We evaluated the inhibition of rotation for BB2-50F, HM2-16F and phenamil while varying the
108 concentration of external sodium to test for Na^+ competitive effects (17). Compounds were tested at
109 concentrations of 1−10 μM using motility buffers containing 1, 5, 20, and 85 mM Na^+. No significant
110 differences in inhibition were observed for HM2-16F and BB2-50F at the Na^+ concentrations tested
111 (Fig. 1D). Inhibition was generally flat for BB2-50F between 0-7.5 μM, with a sharp drop seen at
112 10 μM, whereas HM2-16F inhibition showed a more gradual effect across the range of concentrations
113 tested. In contrast, an exponential decay was seen for phenamil across the concentration range, with the
114 fitted decay constant indistinguishable at all sodium concentrations (Fig 1D, left).

115 ***Activity against phenamil-resistant variants and the proton powered MotA/MotB complex***

116 To assess whether the inhibition of rotation was affected by point mutations known to confer resistance
117 to phenamil, we tested BB2-50F and HM2-16F against known phenamil-resistant mutant constructs at
118 1, 10 and 100 μM using the tethered cell assay. Four different stator mutants were tested in SYC35:
119 PomA(D148Y) PotB, PomA PotB(P16S), PomA(D148Y) PotB(P16S) and PomA PotB(F22Y/L28Q)
120 (68, 69). Phenamil at 10 μM exhibited no significant effect on the resistant strains (Fig. 2A). In contrast,
121 both compounds showed significant inhibition, completely stopping motility at 10 μM in all
122 phenamil-resistant strains (Fig. 2BC).

123 To further profile the specificity of the inhibitors, we evaluated BB2-50F and HM2-16F against the
124 proton-powered stator complex (MotAMotB) in SYC35. Both HM2-16F and BB2-50F reduced rotation
125 of the proton-powered motor at 10 μM and completely inhibited rotation at 100 μM (Fig. 2). In contrast,
126 phenamil did not inhibit MotAMotB stators at concentrations up to 100 μM (Fig. 2).

127 ***Inhibition of motility in other bacterial strains***

128 Inhibition of motility by BB2-50F and HM2-16F was tested in three additional bacterial strains using a
129 free swimming assay that measures the speed of individual cells by videography(25).
130 We first demonstrated inhibition of swimming in MotAMotB and PomAPotB expressing cells
131 (Fig. 3AB), followed by three additional strains: uropathogenic *E. coli* (UPEC)(26) (Fig. 3C), an
132 attenuated enterohemorrhagic *E. coli* (EHEC)(27, 28) (Fig. 3D) and a native sodium swimmer
133 *Vibrio alginolyticus* (29) (Fig. 3E). Both BB2-50F and HM2-16F significantly reduced swimming speed
134 at 10 μM in all strains ($p < 0.05$ in all cases).

135 ***Characterising mechanism of motility inhibition***

136 The activity of BB2-50F and HM2-16F was measured in a bead rotation assay using 1 µm polystyrene
137 bead attached to sticky flagellar filament of JHC36 (Δ*motAmotB* Δ*cheY fliC*^{sticky}). This approach reduced
138 the potential for confounding factors that may have affected the tethered cell assay, such as cell-surface
139 adhesion, while also allowing examination of rotation at lower load and at higher speed.
140 Phenamil reduced PomAPotB-driven rotation from 98 ± 7 Hz at 0 µM to 7± 3 Hz at 10 µM (Fig. 4A),
141 but had no effect on the proton powered MotAMotB (Fig. 4D). In contrast, BB2-50F and HM2-16F
142 reduced the rotation speed of both sodium powered (PomAPotB) and proton powered (MotAMotB)
143 motors to zero at 10 µM (Fig. 4BCF).

144 To assess whether the effects of HM2-16F or BB2-50F were due to direct targeting of the stator
145 complex, we measured rotational diffusion in the presence of drug using the statorless strain.
146 This approach allowed interrogation of whether the compounds were targeting another component of
147 the flagellar motor such as the LP ring or bushing to inhibit rotation. Rotational diffusion for statorless
148 cells remained free in the presence of 10 µM phenamil, indicating no effect on non-stator proteins
149 (Fig. 4G). However, the position of the bead was fixed with minimal rotational or spatial diffusion in
150 the presence of 10 µM BB2-50F (Fig.4H) and HM2-16F (Fig. 4I). This suggested a difference in the
151 mode of action of HM2-16F and BB2-50F compared to phenamil, as these compounds appeared to lock
152 the rotational movement of a 1 µm PS bead.

153 To reduce the possibility of measurements being influenced by lingering surface effects from these
154 comparatively large beads, we reduced bead size and composition, and thus mechanical load, by using
155 a 60 nm gold-nanoparticle attached directly to a straightened hook (30). Given the smaller size of the
156 gold bead, and the straightened hook, this system removed possible bead-cell interactions that may have
157 influenced the earlier PS bead assays. Furthermore, the gold nanoparticle assay allows precise
158 measurement of rotation speed at a load close to zero, providing more direct measure of rotor/stator
159 dynamics free from signal damping caused by viscous drag and mechanical loading (31, 32).
160 For this experiment, we used plasmids expressing proton-powered stator
161 MotAMotB (either pSYC28 or pYC409) and the sodium-powered stator PomAPotB (pSHU1234) in
162 SHU174 (Δ*motAmotB* Δ*fliC* Δ*cheY flgE*$_{+GSS+3Cys}$ *fliK2798*). The gold nanoparticle measurements
163 indicated that there was no effect of the compounds on motor rotation in either strain at 10 µM (Fig 5D
164 and 5H). However, complete inhibition of rotation was seen for BB2-50F at 100 µM in both systems;
165 the rotation speed was reduced from 770 ±115 Hz to 0 Hz (Fig 5B) and from 270 ± 25 Hz to 0 Hz (Fig.
166 5D)
167 in PomAPotB and MotAMotB motors respectively. In contrast, HM2-16F did not reduce rotation in
168 either strain up to 100 µM (Fig. 5F and 5H). This result suggests that both BB2-50F and HM2-16F do
169 not directly target the bushing or the rod of the BFM. Upon observing this, tethered cell assays were
170 repeated in the presence of 0.02% w/v Tween-20 to test whether detergent could remove possible
171 hydrophobic interactions between the bead and cell surface that might underlie the broad antimotility

172 effect, but no reduction in inhibition was observed (Supplementary Fig. 2).
173 Overall, this suggests that the effect was not an artefact of
174 non-specific interactions between the bead and cell-surface in the presence of each inhibitor. In contrast,
175 phenamil significantly reduced the rotation speed of PomAPotB containing cells in the gold bead assay
176 at 10 μM (Fig. 5A), in accordance with its direct, non-competitive mode of inhibition described
177 previously.

178 ***Fluorescence of HM2-16F***

179 We expected HM2-16F in particular to have improved fluorescence properties relative to phenamil due
180 to the additional benzofuran group conjugated to the pyrazine. We measured excitation and emission
181 spectra (Supplementary Fig. 4A), and imaged cells in epifluorescence to observe staining with 10 μM
182 HM2-16F (Supplementary Fig. 4B). We further tested HM2-16F using lifetime fluorescence imaging
183 as the quantum yield appeared low (unsuitable for single molecule imaging). We found that the
184 fluorescence lifetime of HM2-16F was 5.4 ± 0.1 ns, enabling clear resolution against cellular
185 autofluorescence (1.5 ± 0.1 ns) (Supplementary Fig. 4C).

186

187 **Discussion**

188 Motility is a potential target for new anti-virulence agents (33). Inhibitors are expected to exert less
189 selective pressure than current antibiotics (34), and typically inhibit bacteria at lower concentrations
190 than conventional antibiotics (35). This potentially allows more specific pathogen targeting (e.g. sodium
191 only) as well as lower dosage requirements. Amiloride and its analogues are the best known inhibitors
192 of sodium driven bacterial flagellar motors (16, 17, 36, 37). In this study, we evaluated the anti-motility
193 activity of two new amiloride derivatives, BB2-50F and HM2-16F using four methods: 1) tethered cell
194 rotation; 2) free-swimming, 3) 1 μm bead rotation, and 4) 60 nm gold bead rotation.

195 Complete inhibition of sodium-driven bacterial rotation was observed at 10 μM for BB2-50F,
196 HM2-16F and phenamil, indicating that these compounds show similar potency. The new compounds
197 showed better anti-motility activity at lower concentrations than other reported motility inhibitors for
198 sodium powered motor system, e.g. amiloride and arginine (16, 38). Furthermore, the inhibitory effect
199 of both BB2-50F and HM2-16F (Fig 1D) appeared to be sodium independent, implying that both
200 compounds worked in a non-competitive manner like phenamil, but unlike the Na^+ competitive parent
201 amiloride (17). In addition to its activity at low concentrations, HM2-16F also showed increased green
202 fluorescence properties relative to phenamil, enabling the use of epifluorescence and lifetime imaging
203 to measure uptake and release of HM2-16F in treated cells (Supplementary Fig. 4).
204 This finding bolsters its potential applications in, for example, infection diagnostics (39).

205 BB2-50F and HM2-16F did not affect cellular growth at the motility-blocking concentration of 10 μM
206 (Supplementary Fig. 1). Previously a similar result was reported for the motility inhibitor carvacrol,
207 where even at concentrations up to 200 μM, growth remained uninhibited. (35). Restoration of motility
208 following washing supported their non-lethality and reversible inhibition properties.
209 HM2-16F at 100 μM slowed bacterial growth over the first five hours but was no different from
210 untreated cells after 15 hours (Supplementary Fig. 1). In contrast, BB2-50F was toxic at 100 μM,
211 completely inhibiting growth, and likely explaining its consistent anti-motility effect at these
212 concentrations in multiple strains. However total inhibition of rotation in tethered cell assays was
213 observed at a concentration 10-fold lower than this, where no adverse effects on growth were observed
214 (Supplementary Fig. 1). Additionally, BB2-50F and HM2-16F both inhibited phenamil-resistant stator
215 mutants in *E. coli*, and native stators in other strains, both Na^+ and H^+ powered. This property represents
216 an improvement over other reported proton-powered motility inhibitors that are effective only in *E. coli*
217 and require high concentrations (up to 600 μM) (40).

218 The mechanism of action of these compounds and the reason(s) for their anti-motility activity across
219 multiple bacterial strains is not clear. The tethered cell assay is an excellent approach for measuring
220 variations in the response of individual cells to treatment and for initial compound screening, however
221 it does not provide positional information for the rotor or assess performance at low load (41).
222 To examine the mechanism of inhibition, and to rule out potentially confounding cell-surface effects
223 that may have influenced earlier experiments using tethered cells, we used a 1 μm polystyrene bead
224 assay (42) to examine the effects of BB2-50F and HM2-16F on rotation. We observed that phenamil in
225 some instances slowed, but did not stop, rotation, whereas BB2-50F and HM2-16F periodically stopped
226 rotation (Fig. 4). We further examined the effect on statorless constructs (Fig. 4GHI) and noted that
227 phenamil had no effect on rotational diffusion in the absence of stators, whereas BB2-50F and
228 HM2-16F locked free rotational diffusion of the bead. The likely explanation is that phenamil directly
229 associates with the stator complex, reducing active torque generation when bound, and thus has no
230 effect in the absence of stators. In contrast, the two compounds appear to jam the motor or adhere the
231 bead to the cellular surface, creating transient pauses, or complete stops at higher concentrations.

232 To gain further insight into the possible mode of the novel inhibitors, we then employed the highest
233 resolution assay currently available for rotation, a 60-nm gold-nanoparticle affixed directly to a
234 straightened hook (30). The smaller gold nanoparticle, attached to a straightened hook of ~115 nm
235 length, should not interact with cell surface due to the size of the particle and its distance from the cell
236 exterior. Thus, any observed inhibition would potentially indicate drug binding to the LP ring or bushing
237 of the flagellar motor. However, no inhibition of the rotation speeds of the tested strains were seen in
238 the gold bead assay with BB2-50F or HM2-16F at 10 μM, indicating that the effect of both compounds
239 was likely not due to an on-target interaction with the motor. The interaction is presumably not,
240 however, a simple consequence of hydrophobic interactions between the compounds and cells, as the

use of detergent had no effect on the potency of BB2-50F and HM2-16F in inhibiting rotation in theterd cell assays (Supplementary Fig. 2).

Conclusions

We have identified two new amiloride analogues with anti-motility effects at 10 µM concentration in multiple bacterial strains. Whilst the exact mechanism of action of each proved elusive, both compounds were able to inhibit motility in known phenamil-resistant mutants. We have used a wide range of biophysical techniques to rule out possible mechanisms of action: these compounds do not target the stators, the LP ring, or the bushing. Future work can integrate fluorescence measurements with these compounds, and other new derivatives, for targeted drug discovery that aids flagellar research and the development of novel antimicrobials.

Material and Methods:

Chemical:

5-(*N*,*N*-hexamethylene)amiloride (HMA) (UOW), HM2-16F (UOW) and BB2-50F (UOW) were synthesised as described previously (23, 24). Phenamil methanesulfonate salt (Sigma-Aldrich), Chloramphenicol (Sigma-Aldrich), Dimethyl sulfoxide (DMSO) (Sigma-Aldrich) and D-Arabinose (Sigma-Aldrich).

Bacterial Strains and Plasmids and Growth Conditions

The bacterial strains and plasmids used in this study are shown in full in Supplementary Table 1. The primary *E. coli* strains used in this work are SYC35 and RP6894. Pathogenic strains include *Vibrio alginolyticus,* Enterohemorrhagic *Escherichia coli* (EHEC) and Uropathogenic *Escherichia coli* (UPEC). All the strains were cultured in LB broth and LB agar [1% (w/v) Bacto tryptone, 0.5% (w/v) Bacto yeast extract, 0.5% (w/v) NaCl, and 2% (w/v) Bacto agar for solid media] at 37°C. According to the selective antibiotic resistance pattern of the plasmids, chloramphenicol (CAM), ampicillin (AMP) or kanamycin (KAN) were added to a final concentration of 25 µg/mL, 50 µg/mL, and 25 µg/mL, respectively. The *V. alginolyticus* strain, NMB136, was grown in VPG medium (1% (w/v) polypeptone, 0.4% (w/v) K_2HPO_4, 3% (w/v) NaCl, 0.5% (w/v) glycerol) and was washed by TMN85 (85 mM NaCl, 215 mM KCl, 50 mM Tris-HCl (pH 7.5), 5 mM $MgCl_2$, 5 mM glucose) with appropriate inhibitors.

Tethered cell assay:

We measured the rotation speed of the test strains in the presence of different concentration of test compounds and control drugs using tethered cell assays following a previous protocol with some

273 modifications (44). *E. coli* strain SYC35 (Δ*motAmotB fliC*^{sticky}) containing plasmids encoding sodium
274 powered PomAPotB (pSHU1234), proton powered MotAMotB (pDB108) and phenamil resistant
275 PonAPotB (pSHU1235, pSHU1236, pSHU1237, and pSHU1249) were inoculated into TB broth [1%
276 (w/v) Bacto tryptone, 0.5% (w/v) NaCl] containing 0.02% (w/v) arabinose and 25 μg/ml
277 chloramphenicol and were grown overnight (17 h) with 180 rpm at 30 °C. The overnight cultures were
278 sub-cultured with a 50-fold dilution into fresh TB broth and incubated for 5 h with 180 rpm at 30°C to
279 get more motile cells. At OD_{600} ~0.80, the flagella of the cells were sheared by passing the culture
280 multiple times (~35) through a 26G needle syringe. After shearing the flagella, the cells were washed
281 three times with motility buffer [10 mM potassium-phosphate, 10 mM lactic acid, 100 mM NaCl, and
282 0.1 mM EDTA, pH 7.0]. Cells were then attached on tunnel slides and washed sequentially with motility
283 buffer that contained different concentration test compounds (0, 1, 2.5, 5, 7.5, 10, and 100 μM).
284 According to the experiment purpose we used different concentrations NaCl in the motility buffer. The
285 rotational speed of the cells was observed using phase-contrast microscopy (Nikon) and was recorded
286 at 20 frames per second (FPS) through the 40X objective with a camera (Chameleon3 CM3, Point Grey
287 Research). Rotational motion of the cells was analysed using Lab view 2019 software (National
288 Instruments).

289 **Growth Curve Assays**

290 Growth assays were performed in the presence of predetermined concentration of test compound to
291 evaluate the effect of the compounds on bacterial growth following the previous protocol (45) with
292 slight modification. *E. coli* strain SYC35 transformed with sodium powered (PomAPotB) and
293 protonpowered (MotAMotB) was used. Briefly, overnight cultures of the test strains with OD_{600} 1.0
294 were diluted 1:100 in 96-well plates (Corning) with fresh LB broth containing different concentrations
295 of HM2-16F and BB2-50F and incubated at 37°C. Plasmid containing strains (pSHU1234 and pDB-
296 108) were grown in presence of 0.02% (w/v) arabinose and 25 μg/mL chloramphenicol, whereas EHEC
297 and UPEC were grown in LB without arabinose or antibiotic. The OD_{600} were measured in a microplate
298 reader (FLUOstar OPTIMA, BMG LABTECH) every hour for 15 h with a brief shaking interval before
299 each measurement. Measurements in 10 μM were repeated and averaged over three measurements,
300 measurements for 100 μM were repeated and averaged over six measurements.

301 **Polystyrene bead assay:**

302 Briefly, *E. coli* strain JHC36 (Δ*motAmotB* Δ*cheY fliC*^{sticky}) transformed with plasmids encoding sodium
303 powered (PomAPotB) and proton powered (MotAMotB) was grown overnight in TB broth and then
304 sub-cultured with a 50-fold dilution into fresh TB broth and incubated for 5 h with 180 rpm at 30°C to
305 get more motile cells. At OD_{600} ~0.80, the flagella of the cells were sheared by passing the culture
306 multiple times (~35) through a 26G needle syringe. After shearing the flagella, the cells were washed
307 three times with motility buffer [10 mM potassium-phosphate, 85 mM NaCl, and 0.1 mM EDTA, 1%

308 DMSO, pH 7.0]. Then, the glass slide was coated with poly-L-lysine (PLL) (Sigma Aldrich) and
309 incubated for 10 mins and washed with motility buffer and flushed with 1 µm polystyrene bead
310 (Polysciences, Inc) solution. The sample was then washed with motility buffer containing test
311 compound (10 and 100 µM) and the rotational speed was recorded and analyzed using Lab view 2019
312 software (National Instruments).

313 **Gold-nanoparticle assay:**

314 We used the 60 nm gold-nanoparticle assay to get the more accurate flagellar rotation speed at lowered
315 load using the previous protocol (30) with slight modification. Briefly, the SHU174 *E. coli*
316 (Δ*motAmotB* Δ*fliC* Δ*cheY flgE*$_{+GSS+3Cys}$ *fliK2798*) containing plasmids encoding stators was grown and
317 washed with motility buffer [10 mM potassium-phosphate, 10 mM lactate-Na, 67 mM NaCl, 0.1 mM
318 EDTA, 1% DMSO, pH 7.0] and prepared as a cell suspension. The cell suspension was later added to
319 the precipitation of gold nano particle (BBI solutions) and incubated for 30 min. After incubation, the
320 cell mixture was washed with motility buffer and put into PLL coated glass chamber. The sample was
321 then washed with motility buffer containing test compound (10 and 100 µM) and the rotational speed
322 was recorded and analyzed using Lab view 2019 software (National Instruments).

323 **Evaluation of fluorescence property of HM2-16F:**

324 The fluorescence of HM2-16F was analysed using fluorescence microscopy. The emission and
325 excitation spectra of the drug was measured using a spectrophotometer (Cary Eclipse). Briefly, the
326 overnight culture of *E. coli* SYC35 strain transformed with pSHU1234 was prepared and washed with
327 motility buffer. Later, the cell suspension was added to PLL-coated glass slide and incubated for
328 10 mins and again washed with motility buffer. Cells were treated with test compounds by washing
329 with test compound (10 and 100 µM) containing motility buffer. Finally, drug treated cells were imaged
330 in epifluorescence mode using a Elyra Microscope (Zeiss) using a Plan-Apochromat 63x/1.40 Oil DIC
331 M27 objective, 405 nm illumination and BP495-575 + L750 filter sets. Lifetime imaging was executed
332 on Picoquant MicroTime 200 STED equipped with a PMA Hybrid Series Hybrid Photomultiplier
333 Detector. Illumination was provided by 405 nm laser (Diode 450), with a 60x/1.2 UPlanSApo Water
334 Objective.

335 **AUTHOR CONTRIBUTIONS**

336 MIM, JB, PR, BJB and MABB designed and executed experiments in, medicinal chemistry,
337 microbiology, microscopy, and rotational measurement. JL and MIM, MJK, BJB, MABB executed
338 initial compound screening. TI and YS designed and executed experiments in rotational measurement
339 with polystyrene beads and gold nanoparticles. MABB and BJB supervised the design, execution and
340 writing of the project. All authors contributed to writing and revision of the manuscript.

341

342 **ACKNOWLEDGEMENTS**

343 We would like to thank Tohru Minamino, Yong-Suk Che, Myu Yoshida and Rie Ito for helping a
344 construction of strains and plasmids. We would like to thank Jai Tree for providing the EHEC and
345 UPEC strains and thank Seiji Kojima and Michio Homma for providing *V. alginolyticus* strain.

346

347 **FUNDING**

348 MJK was supported by Australian National Health and Medical Research Council (NHMRC) Project
349 Grant (APP1100432). YS was supported by JSPS KAKENHI (JP18H02475 and JP20K06564),
350 MEXT KAKENHI (JP19H05404) and Takeda Science Foundation. BJB acknowledges salary support
351 from the Illawarra Cancer Carers. MABB was supported by a UNSW Scientia Research Fellowship, a
352 CSIRO Synthetic Biology Future Science Platform 2018 Project Grant, and ARC Discovery Project
353 DP190100497.

354

355 **References:**

356 1. Duan Q, Zhou M, Zhu L, Zhu G. 2013. Flagella and bacterial pathogenicity. J Basic Microbiol
357 53:1–8.

358 2. Armitage JP. 2007. Bacterial TaxisEncyclopedia of Life Sciences.

359 3. Berg HC. 2008. E. coli in Motion. Springer Science & Business Media.

360 4. Sowa Y, Berry RM. 2008. Bacterial flagellar motor. Q Rev Biophys 41:103–132.

361 5. Xiu P, Liu R, Zhang D, Sun C. 2017. Pumilacidin-Like Lipopeptides Derived from Marine
362 Bacterium Bacillus sp. Strain 176 Suppress the Motility of Vibrio alginolyticus. Appl Environ
363 Microbiol 83.

364 6. Yang Q, Defoirdt T. 2015. Quorum sensing positively regulates flagellar motility in pathogenic
365 Vibrio harveyi. Environ Microbiol 17:960–968.

366 7. Black RE, Levine MM, Clements ML, Hughes TP, Blaser MJ. 1988. Experimental
367 Campylobacter jejuni Infection in Humans. J Infect Dis 157:472–479.

368 8. Josenhans C, Suerbaum S. 2002. The role of motility as a virulence factor in bacteria. Int J Med
369 Microbiol 291:605–614.

370 9. Kao C-Y, Sheu B-S, Wu J-J. 2016. Helicobacter pylori infection: An overview of bacterial
371 virulence factors and pathogenesis. Biomed J 39:14–23.

372 10. Arslan-Aydoğdu EÖ, Kimiran A. 2018.
373 http://www.scielo.br/scielo.php?script=sci_abstract&pid=S1517-
374 83822018000100189&lng=en&nrm=iso&tlng=en. Braz J Microbiol 49:189–199.

375 11. Kao CY, Lin WH, Tseng CC, Wu AB, Wang MC, Wu JJ. 2014. The complex interplay among
376 bacterial motility and virulence factors in different Escherichia coli infections. Eur J Clin
377 Microbiol Infect Dis 33:2157–2162.

378 12. DRAKE D, MONTIE TC. 1988. Flagella, Motility and Invasive Virulence of Pseudomonas
379 aeruginosa. Microbiology, 134:43–52.

380 13. Allen-Vercoe E, Sayers AR, Woodward MJ. 1999. Virulence of Salmonella enterica serotype
381 Enteritidis aflagellate and afimbriate mutants in a day-old chick model. Epidemiol Infect
382 122:395–402.

383 14. McCarter LL. 2001. Polar Flagellar Motility of theVibrionaceae. Microbiol Mol Biol Rev
384 65:445–462.

385 15. Simchowitz L, Cragoe EJ. 1986. Inhibition of chemotactic factor-activated Na+/H+ exchange in
386 human neutrophils by analogues of amiloride: structure-activity relationships in the amiloride
387 series. Mol Pharmacol 30:112–120.

388 16. Sugiyama S, Cragoe EJ, Imae Y. 1988. Amiloride, a specific inhibitor for the Na+-driven
389 flagellar motors of alkalophilic Bacillus. J Biol Chem 263:8215–8219.

390 17. Atsumi T, Sugiyama S, Cragoe EJ, Imae Y. 1990. Specific inhibition of the Na(+)-driven
391 flagellar motors of alkalophilic Bacillus strains by the amiloride analog phenamil. J Bacteriol
392 172:1634–1639.

393 18. Guia A, Leblanc N, Bose R. 1995. Effects of phenamil on potassium and calcium channels of
394 guinea pig ventricular myocytes. J Pharmacol Exp Ther 274:649–656.

395 19. Kojima S, Asai Y, Atsumi T, Kawagishi I, Homma M. 1999. Na+-driven flagellar motor
396 resistant to phenamil, an amiloride analog, caused by mutations in putative channel components.
397 J Mol Biol 285:1537–1547.

398 20. Jaques S, Kim Y-K, McCarter LL. 1999. Mutations conferring resistance to phenamil and
399 amiloride, inhibitors of sodium-driven motility of Vibrio parahaemolyticus. Proc Natl Acad Sci
400 96:5740–5745.

401 21. Ishida T, Ito R, Clark J, Matzke NJ, Sowa Y, Baker MAB. 2019. Sodium-powered stators of the
402 bacterial flagellar motor can generate torque in the presence of phenamil with mutations near the
403 peptidoglycan-binding region. Mol Microbiol 111:1689–1699.

404 22. Terada H. 1990. Uncouplers of oxidative phosphorylation. Environ Health Perspect 87:213–218.

405 23. Buckley BJ, Aboelela A, Minaei E, Jiang LX, Xu Z, Ali U, Fildes K, Cheung C-Y, Cook SM,
406 Johnson DC, Bachovchin DA, Cook GM, Apte M, Huang M, Ranson M, Kelso MJ. 2018. 6-
407 Substituted Hexamethylene Amiloride (HMA) Derivatives as Potent and Selective Inhibitors of
408 the Human Urokinase Plasminogen Activator for Use in Cancer. J Med Chem 61:8299–8320.

409 24. Buckley BJ, Majed H, Aboelela A, Minaei E, Jiang L, Fildes K, Cheung C-Y, Johnson D,
410 Bachovchin D, Cook GM, Huang M, Ranson M, Kelso MJ. 2019. 6-Substituted amiloride
411 derivatives as inhibitors of the urokinase-type plasminogen activator for use in metastatic
412 disease. Bioorg Med Chem Lett 29:126753.

413 25. Nishiyama M, Sowa Y. 2012. Microscopic Analysis of Bacterial Motility at High Pressure.
414 Biophys J 102:1872–1880.

415 26. Tree JJ, Ulett GC, Ong C-LY, Trott DJ, McEwan AG, Schembri MA. 2008. Trade-off between
416 iron uptake and protection against oxidative stress: deletion of cueO promotes uropathogenic
417 Escherichia coli virulence in a mouse model of urinary tract infection. J Bacteriol 190:6909–
418 6912.

419 27. Sy BM, Lan R, Tree JJ. 2020. Early termination of the Shiga toxin transcript generates a
420 regulatory small RNA. Proc Natl Acad Sci U S A 117:25055–25065.

421 28. Dahan S, Knutton S, Shaw RK, Crepin VF, Dougan G, Frankel G. 2004. Transcriptome of
422 enterohemorrhagic Escherichia coli O157 adhering to eukaryotic plasma membranes. Infect
423 Immun 72:5452–5459.

424 29. Kojima S, Atsumi T, Muramoto K, Kudo S, Kawagishi I, Homma M. 1997. Vibrio alginolyticus
425 mutants resistant to phenamil, a specific inhibitor of the sodium-driven flagellar motor. J Mol
426 Biol 265:310–318.

427 30. Nakamura S, Hanaizumi Y, Morimoto YV, Inoue Y, Erhardt M, Minamino T, Namba K. 2020.
428 Direct observation of speed fluctuations of flagellar motor rotation at extremely low load close
429 to zero. Mol Microbiol 113:755–765.

430 31. Nord AL, Sowa Y, Steel BC, Lo C-J, Berry RM. 2017. Speed of the bacterial flagellar motor
431 near zero load depends on the number of stator units. Proc Natl Acad Sci 114:11603–11608.

432 32. Wang B, Zhang R, Yuan J. 2017. Limiting (zero-load) speed of the rotary motor of Escherichia
433 coli is independent of the number of torque-generating units. Proc Natl Acad Sci 114:12478–
434 12482.

435 33. Allen RC, Popat R, Diggle SP, Brown SP. 2014. Targeting virulence: can we make evolution-
436 proof drugs? 4. Nat Rev Microbiol 12:300–308.

437 34. Barczak AK, Hung DT. 2009. Productive steps toward an antimicrobial targeting virulence.
438 Curr Opin Microbiol 12:490–496.

439 35. van Alphen LB, Burt SA, Veenendaal AKJ, Bleumink-Pluym NMC, van Putten JPM. 2012. The
440 natural antimicrobial carvacrol inhibits Campylobacter jejuni motility and infection of epithelial
441 cells. PloS One 7:e45343.

442 36. Mohr K. 1993. Amiloride and Its Analogs Unique Cation Transport Inhibitors. Edward J.
443 Cragoe jr., Thomas R. Kleyman, Louis Simchowitz. VCH Weinheim — New York — Basel —
444 Cambridge — Tokyo. Date of publication: December 1992. XV, 388 pages. 62 figures. 25
445 tables. DM 189,—, £ 78,—. Pharm Unserer Zeit 22:273–273.

446 37. McCarter LL. 2004. Dual Flagellar Systems Enable Motility under Different Circumstances.
447 Microb Physiol 7:18–29.

448 38. Atsumi T, Yoshimura F, Sugiyama S. 2006. Arginine inhibits Na-driven flagellar motors of
449 alkaliphilic Bacillus. FEMS Microbiol Lett 256:224–228.

450 39. Stone MRL, Butler MS, Phetsang W, Cooper MA, Blaskovich MAT. 2018. Fluorescent
451 Antibiotics: New Research Tools to Fight Antibiotic Resistance. Trends Biotechnol 36:523–536.

452 40. Adams LA, Sharma P, Mohanty B, Ilyichova OV, Mulcair MD, Williams ML, Gleeson EC,
453 Totsika M, Doak BC, Caria S, Rimmer K, Horne J, Shouldice SR, Vazirani M, Headey SJ,
454 Plumb BR, Martin JL, Heras B, Simpson JS, Scanlon MJ. 2015. Application of Fragment-Based
455 Screening to the Design of Inhibitors of Escherichia coli DsbA. Angew Chem Int Ed 54:2179–
456 2184.

457 41. Nirody JA, Sun Y-R, Lo C-J. 2017. The biophysicist's guide to the bacterial flagellar motor.
458 Adv Phys X 2:324–343.

42. Kasai T, Sowa Y. 2017. Measurements of the Rotation of the Flagellar Motor by Bead Assay. Methods Mol Biol Clifton NJ 1593:185–192.

43. Alcalde-Rico M, Hernando-Amado S, Blanco P, Martínez JL. 2016. Multidrug Efflux Pumps at the Crossroad between Antibiotic Resistance and Bacterial Virulence. Front Microbiol 7.

44. Sowa Y, Homma M, Ishijima A, Berry RM. 2014. Hybrid-fuel bacterial flagellar motors in Escherichia coli. Proc Natl Acad Sci 111:3436–3441.

45. Islam MI, Lin A, Lai Y-W, Matzke NJ, Baker MAB. 2020. Ancestral Sequence Reconstructions of MotB Are Proton-Motile and Require MotA for Motility. Front Microbiol 11.

46. Block SM, Blair DF, Berg HC. 1989. Compliance of bacterial flagella measured with optical tweezers. Nature https://doi.org/10.1038/338514a0.

47. Inoue Y, Lo C-J, Fukuoka H, Takahashi H, Sowa Y, Pilizota T, Wadhams GH, Homma M, Berry RM, Ishijima A. 2008. Torque–Speed Relationships of Na+-driven Chimeric Flagellar Motors in Escherichia coli. J Mol Biol 376:1251–1259.

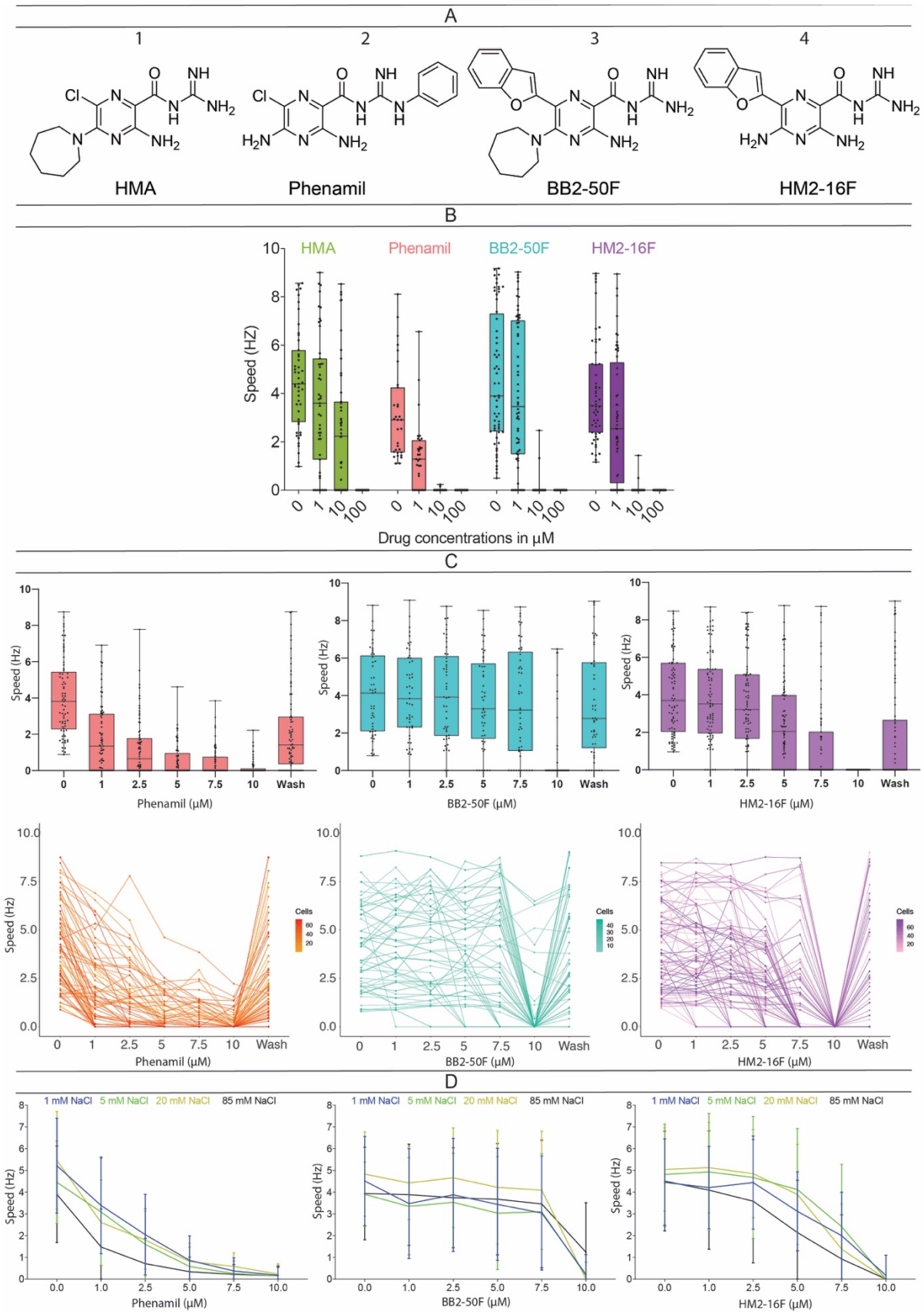

Fig. 1: Structures and effects of compounds on bacterial rotation in tethered cell assays. (A) Chemical structures of controls 5-*N,N*-(hexamethylene)-amiloride (HMA) and phenamil and test

477 compounds BB2-50F and HM2-16F. **(B)** Tethered cell rotation speed (Hz) after treatment with drugs
478 (μM). Cells were *E. coli* SCY35 strain (ΔMotAB, FliC-sticky) with pSHU1234 (pomApotB). Cells
479 were treated with 0, 1, 10 and 100 μM of each compound. Boxes represent the 25th and 75th percentile,
480 with median indicated by dividing line. Whiskers cover the full range from minimum to maximum
481 ($n \geq 30$). The lime green bar = HMA, salmon = phenamil, blue = BB2-50F and violet = HM2-16F. **(C)**
482 Dose characterisation of compounds. Cells were treated with 0, 1, 2.5, 5, 7.5 and 10 μM of each
483 compound. The line graphs (bottom) indicate the tracking of individual cells' change in rotation speed.
484 **(D)** Effects of sodium concentration ($[Na^+]$) on inhibitory activity. Cells were treated with 0, 1, 2.5, 5,
485 7.5 and 10 μM drugs diluted in motility buffer containing different Na^+ concentrations (1, 5, 20 and 85
486 mM). Total ionic concentration was held constant and balanced with 84, 80, 65 and 0 mM KCl
487 respectively.

488

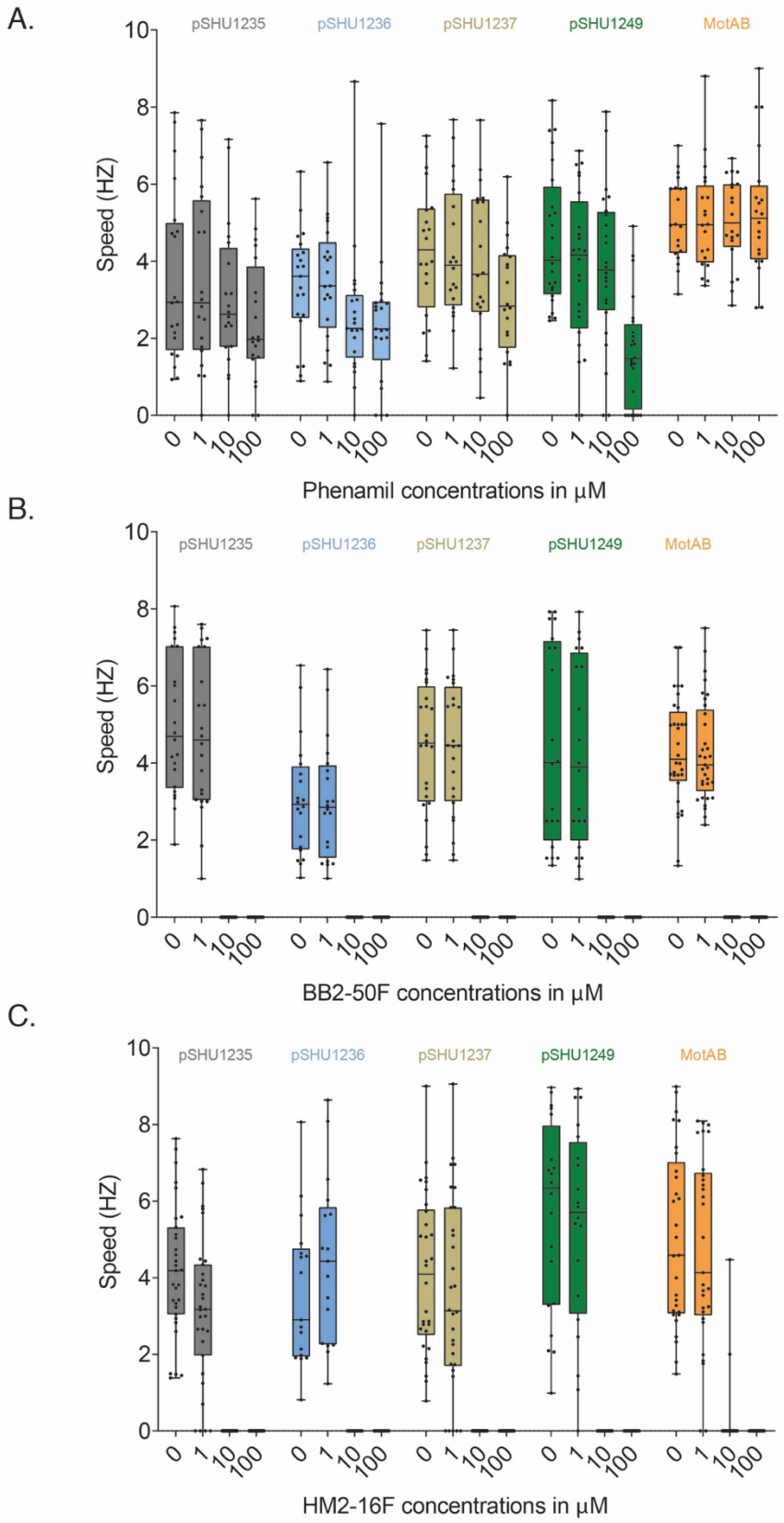

489

490 **Fig. 2:** Activity of compounds against phenamil-resistant stators and proton-powered MotAMotB.
491 Tethered cell speed (Hz) in response to 0, 1, 10, and 100 µM of: **A)** phenamil, **(B)** BB2-50F and

492 (**C**) HM2-16F. Cell used for all assays were *E. coli* SCY35 strain (ΔmotAB, FliC-sticky) with
493 pSHU1235 (PomA (D148Y), PotB), pSHU1236 [PomA, PotB (P16S)], pSHU1237 [PomA (D148Y),
494 PotB (P16S)] and pSHU149 [PomA, PotB (F22Y/L28Q)] and pDB-108 [MotAMotB] respectively.
495 Boxes represent the 25th and 75th percentile, with median indicated by dividing line. Whiskers depict
496 the full range from minimum to maximum ($n \geq 20$).

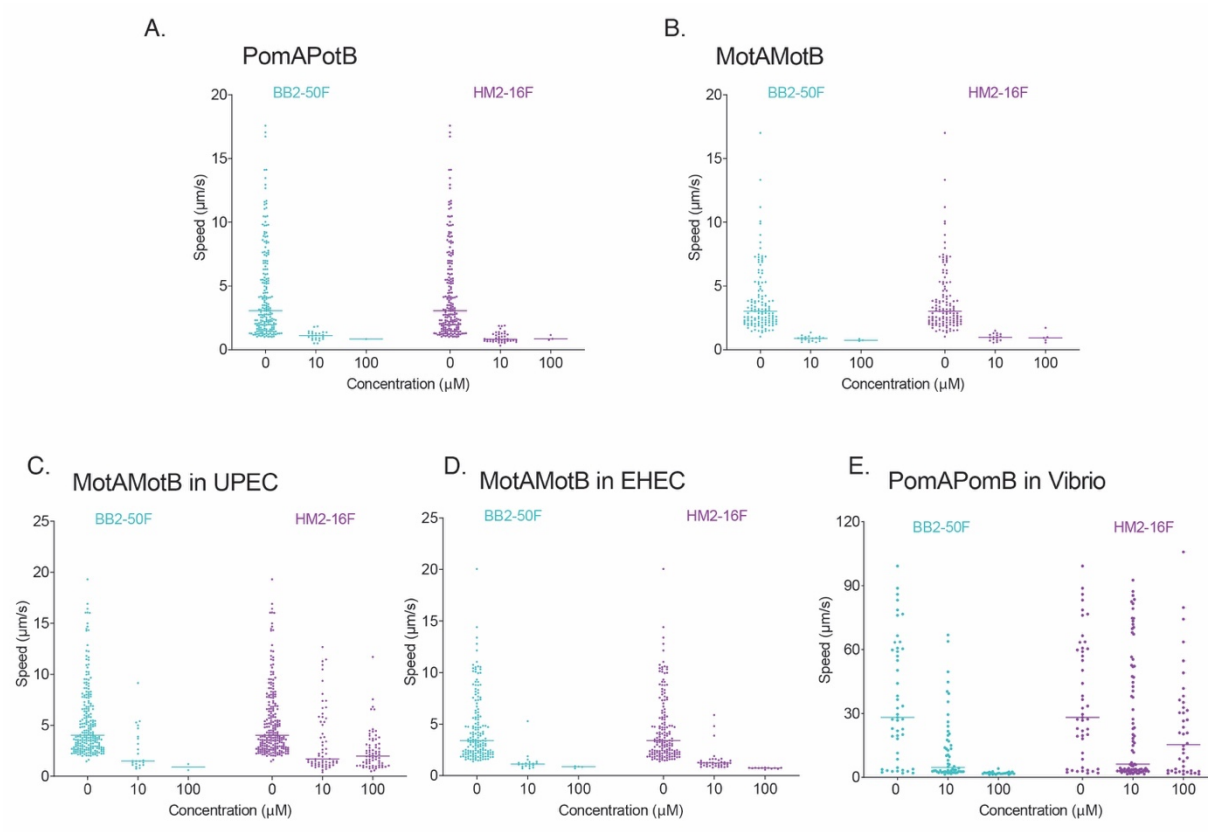

Fig. 3: Inhibition of swimming speed by BB2-50F and HM2-16F. Bacterial swimming speed was measured by tracking individual cells using videography in the presence of different concentrations (0, 10, 100 µM) of each compound. Swimming speed of: **(A)** PomAPotB expressed via plasmid in ΔmotAB strain, **(B)** MotAMotB expressed via plasmid in ΔmotAB strain, **(C)** MotAMotB in uropathogenic *Escherichia coli* (UPEC) and **(D)** MotAMotB in enterohemorrhagic *Escherichia coli* (EHEC), and **(E)** PomAPomB in *Vibrio alginolyticus,* all following wash with drug. Speeds of individual cells shown in µm/s with the scattered plots, median speed indicated by line (n ≥ 30).

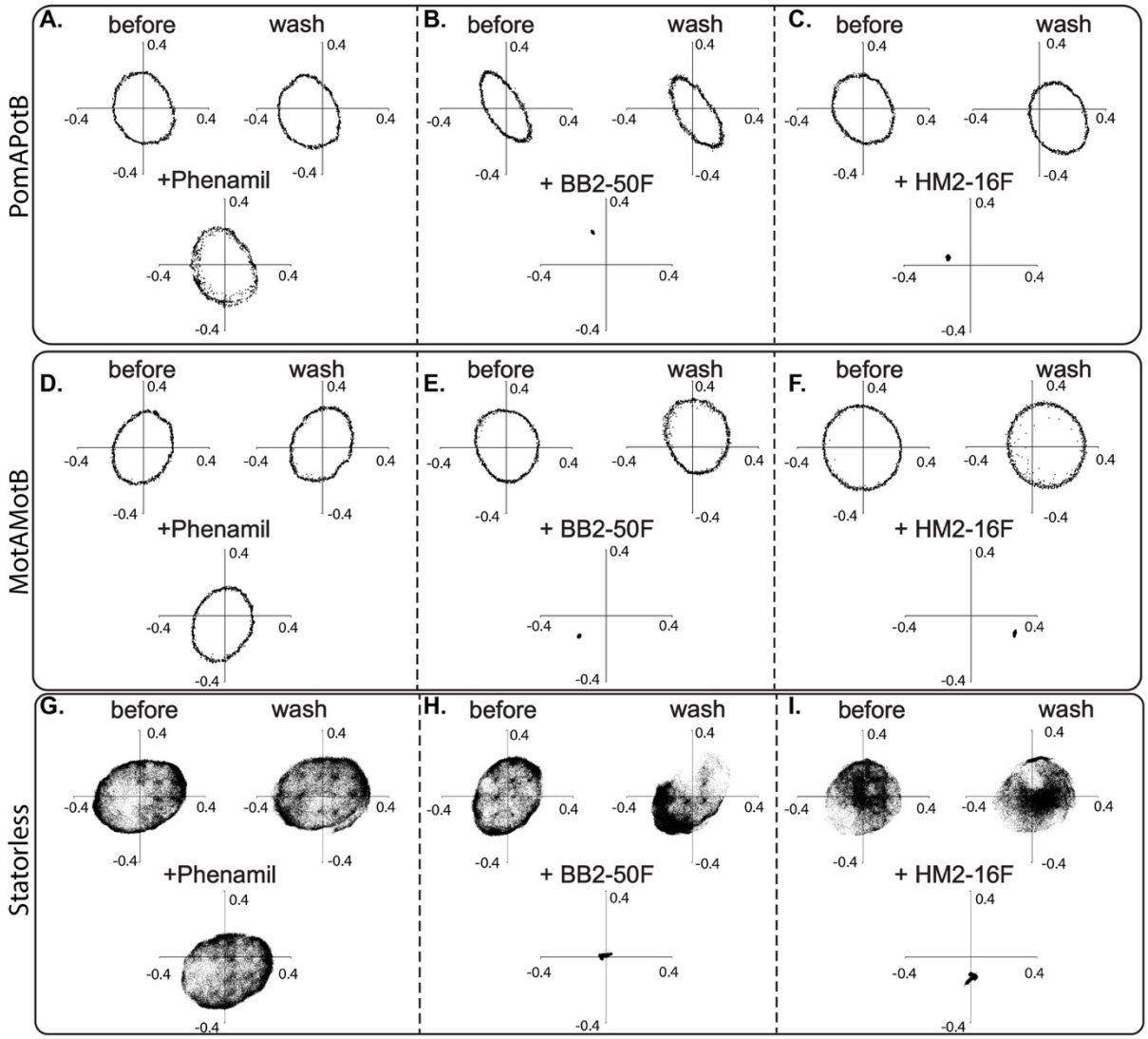

Fig. 4: Bead assay results for phenamil, BB2-50F and HM2-16F. (top) 1 µm Polystyrene bead assay in *E. coli* strain JHC36 with plasmid expressed PomAPotB stator (pSHU1234) in presence of (A) phenamil, (B) BB2-50F and (C) HM2-16F. Each panel shows three X-Y scatter plots (over 1 s) of the position a bead attached to the rotating flagellar filament of a single cell before exposure to drug, after exposure to drug, and after wash to remove drug. Raw speed vs time and XY vs time plots shown in Supplementary Fig. 3. **(middle)** Bead assay in *E. coli* strain JHC36 with plasmid expressed MotAMotB stator in presence of (D) phenamil, (E) BB2-50F and (F) HM2-16F. **(Bottom)** X-Y position (over 60 s) for *E. coli* strain JHC36 with no stators expressed. The Brownian diffusion of the bead for 60-120 s is shown before and after treatment with (G) phenamil, (H) BB2-50F and (I) HM2-16F, respectively. All drugs washed in as 50 µL of 10 µM drug, washed out with 200 µL of 85MTB. All lengths in µm.

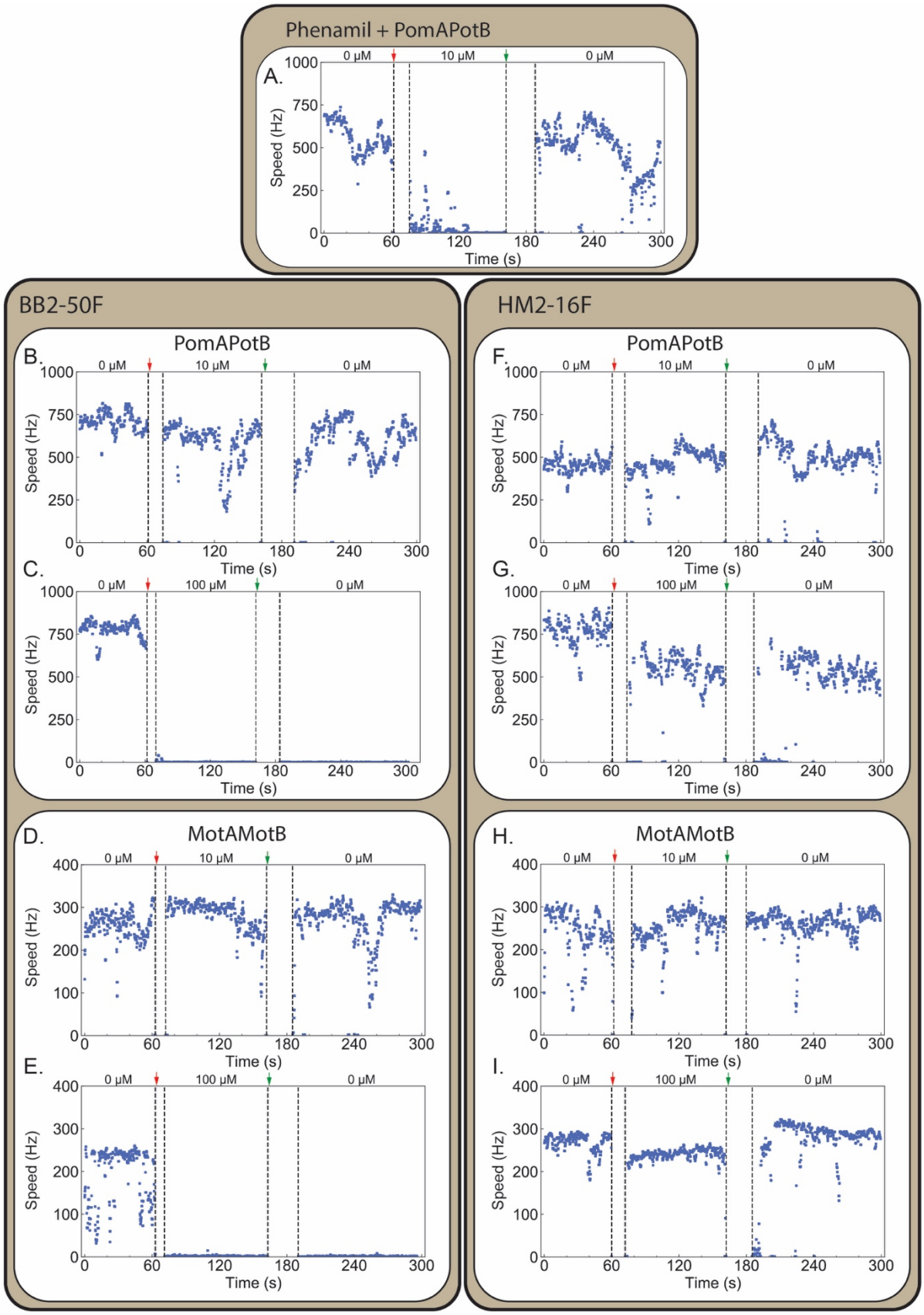

Fig. 5: Gold bead nanoparticle assay results of test compounds. Speed versus time plots for 60 nm gold nanoparticle attached directly to rotating, straightened hook of bacterial flagellar motor before, during and after exposure to drug. Gold nanoparticle assay was performed in SHU174 *E. coli* strain in

523 presence of 10/100 μM BB2-50F (left) and HM2-16F (right) for both PomAPotB and MotAMotB
524 stators, with phenamil action on PomAPotB as a positive control. Red arrow indicates drug flowed in
525 as 50 μL of stated concentration (10 μM or 100 μM), green arrow indicates washout of drug with 200
526 μL of 67MTB. (A) Positive control for 10 μM phenamil against rotation driven by PomAPotB. Left
527 side: BB2-50F against PomAPotB at (B) 10 μM and (C) 100 μM. BB2-50F against MotAMotB at (D)
528 10 μM and (E) 100 μM. Right side: HM2-16F against PomAPotB at (F) 10 μM and (G) 100 μM**.** HM2-
529 16F against MotAMotB at (H) 10 μM and (I) 100 μM.

530

531